Eur Arch Otorhinolaryngol (2015) 272:2371–2379
DOI 10.1007/s00405-014-3353-3

RHINOLOGY

Calculating nasoseptal flap dimensions: a cadaveric study using cone beam computed tomography

Ellen ten Dam · Astrid G. W. Korsten-Meijer · Rutger H. Schepers · Wicher J. van der Meer · Peter O. Gerrits · Bernard F. A. M. van der Laan · Robert A. Feijen

Received: 12 July 2014 / Accepted: 20 October 2014 / Published online: 31 October 2014

Abstract We hypothesize that three-dimensional imaging using cone beam computed tomography (CBCT) is suitable for calculating nasoseptal flap (NSF) dimensions. To evaluate our hypothesis, we compared CBCT NSF dimensions with anatomical dissections. The NSF reach and vascularity were studied. In an anatomical study (n = 10), CBCT NSF length and surface were calculated and compared with anatomical dissections. The NSF position was evaluated by placing the NSF from the anterior sphenoid sinus wall and from the sella along the skull base towards the frontal sinus. To visualize the NSF vascularity in CBCT, the external carotic arteries were perfused with colored Iomeron. Correlations between CBCT NSFs and anatomical dissections were strongly positive ($r > 0.70$). The CBCT NSF surface was 19.8 cm^2 [16.6–22.3] and the left and right CBCT NSF lengths were 78.3 mm [73.2–89.5] and 77.7 mm [72.2–88.4] respectively. Covering of the anterior skull base was possible by positioning the NSF anterior to the sphenoid sinus. If the NSF was positioned from the sella along the skull base towards the frontal sinus, the NSF reached partially into the anterior ethmoidal sinuses. CBCT is a valuable technique for calculating NSF dimensions. CBCT to demonstrate septum vascularity in cadavers proved to be less suitable. The NSF reach for covering the anterior skull base depends on positioning. This study encourages preoperative planning of a customized NSF, in an attempt to spare septal mucosa. In the concept of minimal invasive surgery, accompanied by providing customized care, this can benefit the patients' postoperative complaints.

Keywords Nasoseptal flap · Skull base reconstruction · Preoperative planning · Anatomy · Cone beam computed tomography · Three-dimensional imaging

E. ten Dam (✉) · A. G. W. Korsten-Meijer · B. F. A. M. van der Laan · R. A. Feijen
Department of Otorhinolaryngology/Head and Neck Surgery, University Medical Center Groningen, Hanzeplein 1, 9700 RB Groningen, The Netherlands
e-mail: e.ten.dam@umcg.nl

E. ten Dam
Graduate School of Medical Sciences (Groningen University Institute for Drug Exploration), University of Groningen, Groningen, The Netherlands

R. H. Schepers
Department of Oral- and Maxillofacial Surgery, University Medical Center Groningen, Groningen, The Netherlands

W. J. van der Meer
Department of Orthodontics, University Medical Center Groningen, Groningen, The Netherlands

P. O. Gerrits
Department of Neuroscience Section Anatomy, University Medical Center Groningen, Groningen, The Netherlands

Introduction

The nasoseptal flap (NSF) is often used for endonasal skull base reconstruction [1]. Due to its versatility and reliability, the NSF is known as a work horse for endonasal reconstruction [1–5]. An advantage of the NSF is its endoscopic harvesting, thereby limiting the morbidity of the procedure [6, 7]. Moreover, the NSF decreased the incidence of postoperative cerebrospinal fluid (CSF) leaks to less than 5 % [1, 8, 9]. Preoperative planning of the NSF is difficult because the NSF is designed according to a size and shape of an expected skull base defect. To prevent failure of covering, it is recommended to overestimate the NSF size [1]. It has been shown that the NSF is often width enough

for covering skull base defects by incorporation of nasal floor and/or inferior turbinate mucosa [5, 10]. However, a longer NSF is not possible. The NSF has limited length and can be deficient along the anterior-most part of ventral skull base defects [9, 11].

Clinical experience shows that the NSF is often made too large during surgery. As a result, the undue damage to septal mucosa can potentially lead to an increased postoperative morbidity [7, 12, 13]. In the concept of minimal invasive surgery, accompanied by providing customized care for the patient, preoperative planning of a limited NSF may benefit the postoperative complaints by sparing septal mucosa [3, 7, 12]. Earlier studies demonstrated that preoperative analyses using computed tomography (CT) are helpful in anticipating on skull base defects and subsequent planning an NSF [11, 14]. Compared to CT, cone beam computed tomography (CBCT) combines lower radiation dose and high spatial resolution which results in high-quality three-dimensional (3D) images [15]. Due to these advantages, lower costs and an easier surgery, CBCT is already widely used in maxillofacial surgery and orthodontics [16–18].

Objective. We hypothesize that 3D imaging using CBCT is suitable for calculating NSF dimensions. Therefore, CBCT NSF dimensions were compared with anatomical dissections. We focused on NSF surface and length and not on NSF width because the NSF is often width enough for covering skull base defects in clinical practice [10, 11]. The NSF reach and vascularity were also studied.

Materials and methods

Specimens

Ten fresh frozen human cadaver heads were used to harvest 20 NSFs. Formal approval was granted before starting this study. Exclusion criteria were pre-existing conditions altering the skull base and nasal septum and previous sinus or skull base surgery. Two cadaver heads were used in earlier experiments for planning of sinus floor augmentation without damaging the nasal septum.

Radiological study

CBCT imaging

The cadaver heads were scanned using the same i-Cat scanner (i-Cat, Imaging Sciences International, Hatfield, PA) [18]. The heads were scanned with a 0.3 mm voxel size with a 17 × 23 cm field of view, to mimic the clinical situation [19, 20]. The heads were positioned and fixed in the midline of the scanner, heads facing forward and frankfort horizontal plane parallel to the floor [21].

Segmentation

The CBCT dataset was exported in DICOM multi-file format and imported into SimPlant O&O version 2012 software (Materialise Dental, Leuven, Belgium). A surface model was created using the segmentation settings for "bone". The resulting 3D skull model was set in natural head position by rotating the model around the *X*-, *Y*-, or *Z*-axis. The nasal septum was positioned in the midline according to the coordinate system of the software. A two-dimensional (2D) NSF mask was created by drawing with a "2D mask painting tool" in the sagittal plane overlying the image of the nasal septum, assuring that the borders of the mask coincided with the NSF borders used for dissection (*Sect. 2.3.2*). The mask was converted to a 3D object.

CBCT NSF dimensions

Nasoseptal flap length (NSF-L) was defined as the sum of the pedicle length (P-L) and length of the septal part of the NSF (S-L). The sphenopalatine foramen (SPF) was used as reference point [14, 22]. The SPF was identified in a horizontal and frontal plane of a 2D image. To standardize the SPF opening, two lines were drawn perpendicular to each other in the horizontal plane: (1) one line parallel to the medial maxillary sinus wall and (2) one line parallel to the posterior maxillary sinus wall. The intersection of these two lines was defined as the SPF outlet. The distance between the SPF outlet and the NSF was accepted as P-L (Fig. 1). The projection of SPF (P-SPF) on the nasal septum was identified in the sagittal plane. The S-L was measured as the distance between P-SPF and the most anterior NSF border (Fig. 2). The NSF surface (NSF-S) was automatically calculated using the 'high' quality setting (Fig. 2). To assess the optimal setting for the automatic surface calculation, a 400 × 400 square mask was created. The surface was calculated with 'low', 'medium', 'high', and 'optimal' reconstruction quality settings. The length and width of the square were also measured with the measurement tools present. To ensure proper placement of the measurement points, the edge of the square was magnified 1,000 times while placing points. The difference between the automatic and manually calculated surface was compared for the different reconstruction quality settings. The 'high' quality setting proved to be the most consistent in the automatic surface calculations while providing the smallest difference compared to the manual calculations (mean difference 0.81 cm^2, SD 0.29, range 0.32–1.18).

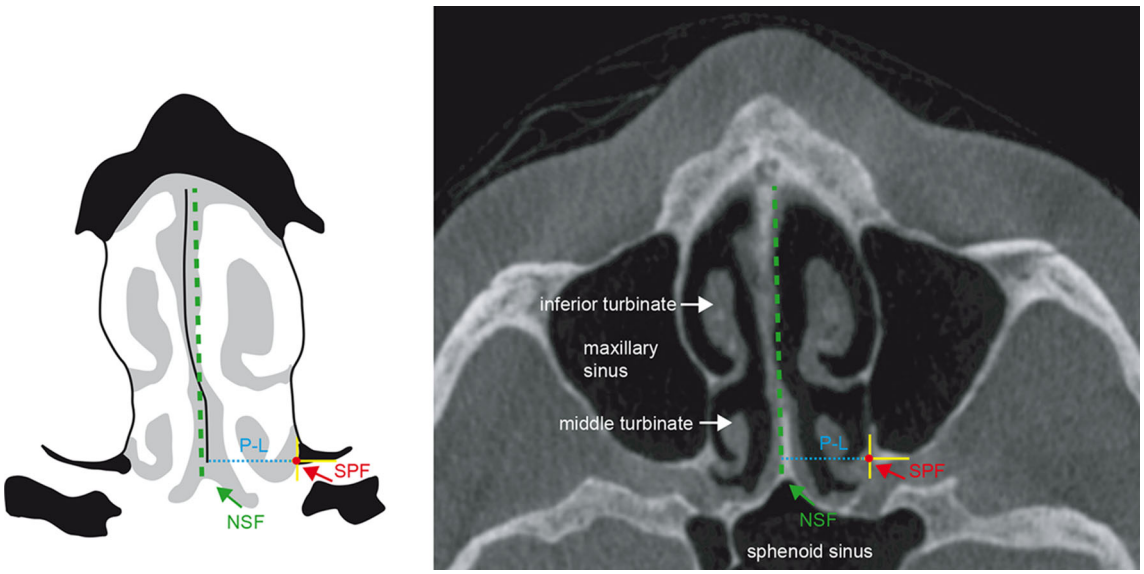

Fig. 1 Drawing of the nose and CBCT image in the axial plane showing the pedicle length (P-L; *dashed blue line*): the distance between the sphenopalatine foramen (SPF; *red dot*) and the nasoseptal flap (NSF; *dashed green line*)

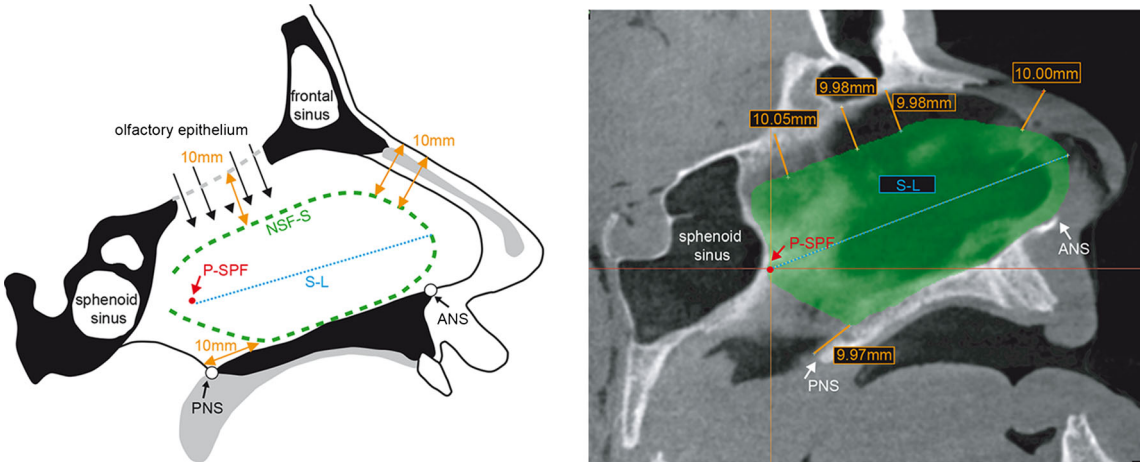

Fig. 2 Drawing of the nose and CBCT image in the sagittal plane showing the design of the nasoseptal flap (NSF), the surface area of the NSF (NSF-S; *dashed green line*), and the length of the septal part of the NSF (S-L; *blue dotted line*): the distance between the projection of the sphenopalatine foramen on the nasal septum (P-SPF; *red dot*) and the most anterior border of the NSF. *ANS* anterior nasal spine, *PNS* posterior nasal spine

Anatomical study

NSF vascularity

A test series of 10 ml syringes filled with contrast enhancers in different concentrations showed that a mixture of Iomeron 350 (X-ray contrast medium containing 350 mg iodine/ml), cadmium red deep acrylic color (Winsor & Newton) and water in a ratio 10:1:1 showed the best visualization using CBCT. For injection of the vascular system, specimens were defrosted at 4 °C during 84 h. Bilaterally, the jugular vein and common carotid artery were identified. The internal carotid artery and external carotid artery branches (superior thyroid artery, lingual artery, facial artery, and ascending pharyngeal artery) were sutured to restrict flow to the maxillary artery. The external carotid artery was cannulated and connected to a 60 ml syringe. The vascular system was pre-rinsed with 60 ml diluted ethylene glycol to remove blood clots. After injection with 40 ml colored Iomeron, the carotid arteries and the jugular veins were sutured. A second CBCT was made to visualize the NSF vascularity. The heads were stored in a freezer at −20 °C.

Table 1 Dimensions of the CBCT NSF and anatomical dissected NSF for males ($n = 6$) and females ($n = 4$)

	Males		Females		Total	
	CBCT	Anatomical	CBCT	Anatomical	CBCT	Anatomical
NSF-L (mm)						
Left	81.1 (73.9–89.5)	80.3 (75.8–83.0)	76.8 (73.2–79.3)	76.1 (73.0–81.2)	78.3 (73.2–89.5)	77.6 (73.0–83.0)
Right	79.6 (73.7–88.4)	79.2 (75.4–81.5)[a]	76.2 (72.2–82.6)	73.9 (71.6–78.9)	77.7 (72.2–88.4)	78.7 (71.6–81.5)
P-L (mm)						
Left	13.4 (11.7–14.4)	12.5 (11.3–16.5)	12.6 (11.8–14.5)	13.0 (11.4–13.3)	13.0 (11.7–14.5)	12.6 (11.3–16.5)
Right	11.9 (10.8–13.7)	12.2 (10.5–13.3)[a]	13.6 (11.3–16.8)	13.0 (12.5–16.2)	12.8 (10.8–16.8)	12.5 (10.6–16.2)
S-L (mm)						
Left	68.6 (61.7–75.4)	66.2 (63.6–69.5)	64.3 (58.7–67.5)	63.8 (59.7–68.5)	66.0 (58.7–75.4)	65.7 (59.7–69.5)
Right	67.0 (62.9–75.8)	66.5 (63.8–69.3)[a]	63.8 (58.3–65.8)	60.9 (59.1–62.8)	64.9 (58.3–75.8)	63.8 (59.1–69.3)
NSF-S (cm^2)	21.3 (18.7–22.3)	19.2 (18.5–24.6)	17.4 (16.6–18.4)	16.7 (16.1–20.3)	19.8 (16.6–22.3)	18.7 (16.1–24.6)

The dimensions are shown as median (range)

CBCT cone beam computed tomography, *NSF* nasoseptal flap, *NSF-L* length of the nasoseptal flap, *P-L* pedicle length, *S-L* length of the septal part of the nasoseptal flap, *NSF-S* surface area of the nasoseptal flap

[a] Median (range) of 5 males instead of 6 males because of technical problems during cutting of one head into the sagittal plane

Dissected NSF dimensions

Frozen specimens were cut sagitally at the level of the medial canthus, corresponding to the entry side of the sphenopalatine artery into the nose. After defrosting for 24 h, the NSF was outlined as described previously [1]. To standardize the NSF design, the inferior incision line was made along the nasal cavity floor from a point 10 mm from the posterior nasal spine to the anterior nasal spine. The superior incision line, 10 mm below the cribriform plate, and the inferior incision line were joined by an incision line following the curvature of the cartilage nasal septum, preserving the most anterior 10 mm. Before harvesting, the NSF-L was measured using a caliper (Mitutoyo, Japan). The P-SPF on the nasal septum was determined by insertion of a needle from the lateral side through the SPF. Photographs of the NSF were imported into ImageJ [23] to calculate the NSF-S.

NSF transposition

The NSF was elevated from the nasal septum in an anterior to posterior direction and from the anterior face of the sphenoid sinus to a level as close as possible to the SPF. The NSF was positioned from the anterior sphenoid sinus wall along the skull base toward the frontal sinus. After removing the anterior wall and a part of the bottom of the sphenoid sinus, the NSF was positioned from the sella along the skull base toward the frontal sinus.

Statistics

SPSS Statistics version 20.0 for Windows (SPSS Inc, Chicago) was used. The NSF dimensions were measured 3 times by 2 independent observers. The agreement between the repeated measurements for the NSF-L was high (ICC > 0.883). All measurements are displayed as median (range). To measure the strength of the linear relationship between the CBCT NSF dimensions and anatomical dissections, Spearman's correlation coefficient r was used. A two-tailed $p < 0.05$ was considered significant.

Results

Characteristics

Ten fresh frozen specimens (6 males, aged 85 years [67–88], and 4 females, aged 73 years [72–86]), were used for 10 CBCT NSF reconstructions and harvesting of 20 NSFs. The ages of three specimens were unknown.

NSF dimensions

CBCT NSF

Length. The left NSF-L was 78.3 mm (73.2–89.5). The P-L was 13.0 mm (11.7–14.5) and the S-L was 66.0 mm (58.7–75.4). The right NSF-L was 77.7 mm (72.2–88.4). The P-L was 12.8 mm (10.8–16.8) and the S-L 64.9 mm (58.3–75.8). Females showed a shorter NSF than males because of a shorter S-L. No difference in P-L was found between males and females.

Surface. The NSF-S was 19.8 cm^2 (16.6–22.3). Males displayed a larger NSF-S compared to females (Table 1).

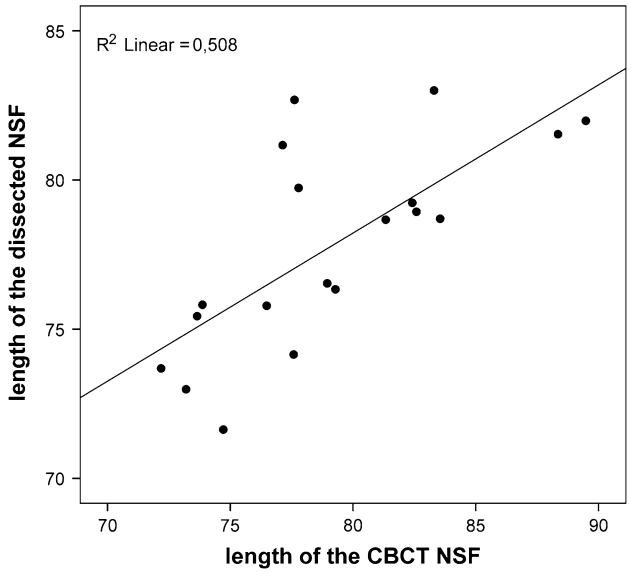

Fig. 3 Correlation between the CBCT NSF length and the anatomical dissected NSF length (mm)

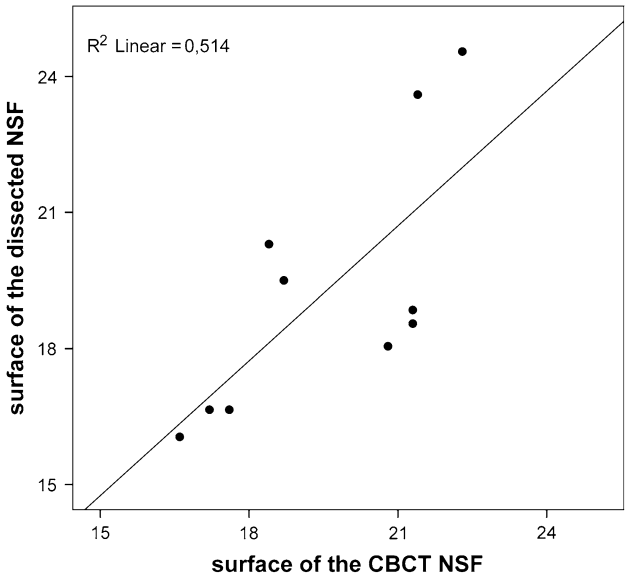

Fig. 4 Correlation between the CBCT NSF surface area and the anatomical dissected NSF surface area (cm^2)

Anatomical dissected NSF

Measurement of the right NSF-L was not possible in case S3 due to technical problems during cutting of the head into the sagittal plane.

Length. The left NSF-L was 77.6 mm (73.0–83.0). The P-L was 12.6 mm (11.3–16.5) and the S-L was 65.7 mm (59.7–69.5). The right NSF-L was 78.7 mm (71.6–81.5). The P-L was 12.5 mm (10.5–16.2) and the S-L was 63.8 mm (59.1–69.3). The NSF-L in females was shorter than in males. In P-L, no difference was found between males and females.

Surface. The NSF-S was 18.7 cm^2 (16.1–24.6). Males displayed a larger average surface than females (Table 1).

Correlations

Comparison between CBCT NSF dimension and anatomical dissections revealed a very strong positive correlation in NSF-L ($r = 0.734$, $p = 0.000$, $N = 19$), P-L ($r = 0.785$, $p = 0.000$, $N = 19$), S-L ($r = 0.777$, $p = 0.000$, $N = 19$), and NSF-S ($r = 0.799$, $p = 0.006$, $N = 10$) (Figs. 3, 4).

NSF transposition

By positioning the NSF from the anterior sphenoid sinus wall along the skull base toward the frontal sinus, the NSF reached into or beyond the frontal recess in all specimens. If the NSF was positioned from the sella along the skull base toward the frontal sinus, it was possible to cover the planum sphenoidale and the posterior ethmoidal sinuses in all specimens (Fig. 5).

NSF vascularity

Injection of colored Iomeron was not possible in two specimens (due to an impaired vascular system and severe atherosclerosis). With CBCT, the course of the maxillary artery and the sphenopalatine artery passing the SPF was visualized (Fig. 6). Branching of the sphenopalatine artery could not be visualized. Cadmium red acrylic color as contrast enhancer enabled visualization of the posterior septal branches of the nasal septum after anatomical dissection (Fig. 7). In most cases, the sphenopalatine artery divided into its terminal branches before reaching the posterior septum. On the nasal septum, the sphenopalatine artery divided into 2 or 3 branches for septal blood circulation.

Discussion

This is the first study comparing CBCT NSF dimensions with anatomical dissections. Our results showed that CBCT is a valuable technique for calculating NSF dimensions. Strong positive correlations were found between CBCT and anatomical dissected NSF dimensions. This encourages preoperative planning of a customized NSF for endonasal reconstruction of skull base defects in an attempt to spare septal mucosa.

We defined the NSF-L as the sum of the P-L and S-L. This is in contrast to other studies reporting only the S-L.

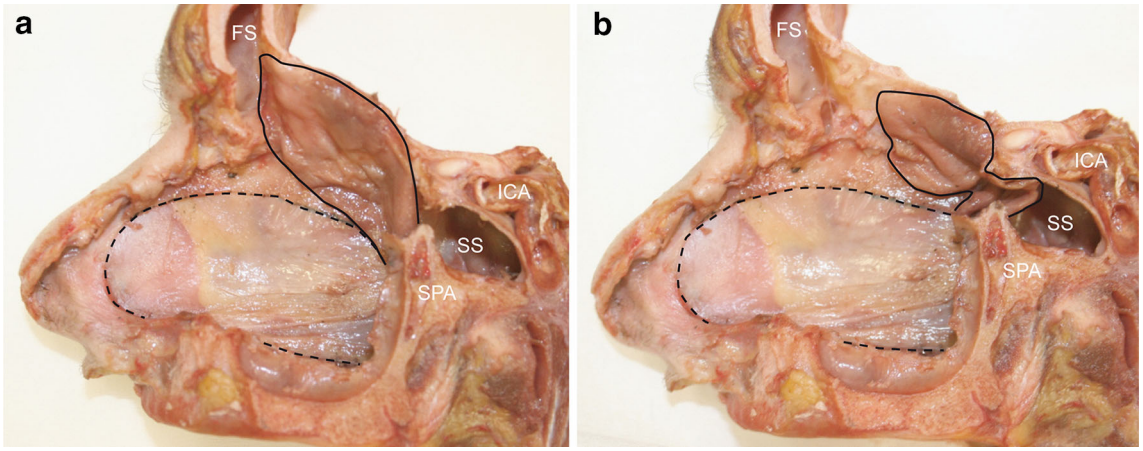

Fig. 5 Sagittal cuts of a cadaveric head showing the transposition of the pedicled nasoseptal flap. **a** Transposition of the nasoseptal flap *(black line)* from the planum sphenoidale beyond the recessus of the frontal sinus. **b** Transposition of the nasoseptal flap (*black line)* from the sella into the anterior ethmoidal sinus. The dashed black lines indicate the outline of the nasoseptal flap incisions. *FS* frontal sinus, *ICA* internal carotid artery, *SS* sphenoid sinus, *SPA* sphenopalatine artery

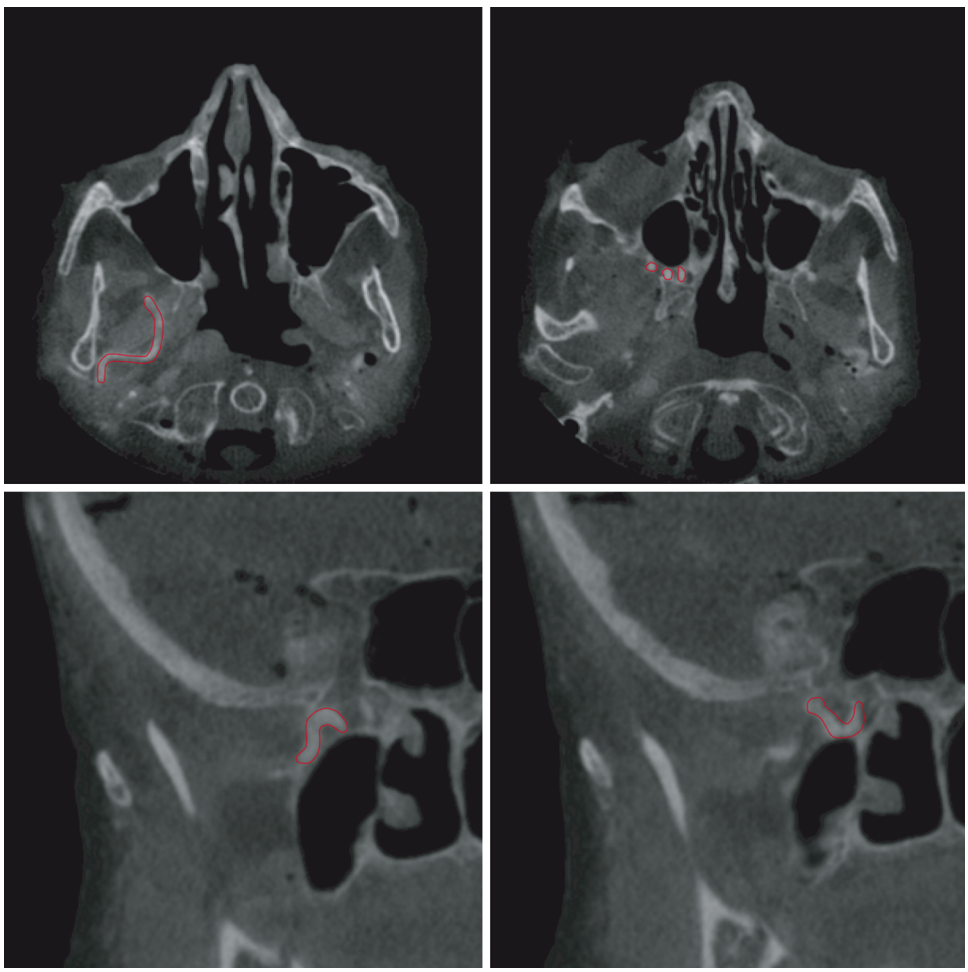

Fig. 6 CBCT enabled visualization of the course of the right maxillary artery and the sphenopalatine artery (*surrounded by a red line*) passing the sphenopalatine foramen in the axial plane (*upper row*) and coronal plane (*bottom row*)

Only one other published study of Pinheiro-Neto et al. [14] calculated a NSF-L of 82 mm, which is in agreement with our CBCT NSF-L. In the same study of Pinheiro-Neto et al. [14], a mean P-L of 10 mm was calculated, whereas we calculated a CBCT P-L of 13 mm. The difference in the calculated P-L may be due to a variation in the

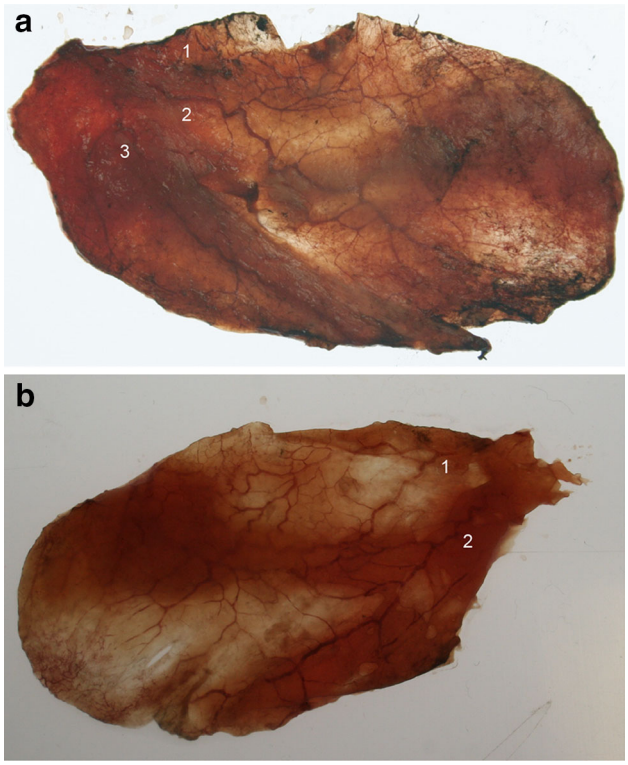

Fig. 7 Injection of the vascular system with cadmium red acrylic color as contrast enhancer enabled visualization of the posterior septal branches of the nasoseptal flap after anatomical dissections. The sphenopalatine artery divided into 3 (**a**) or 2 (**b**) terminal branches before reaching the posterior nasal septum

measurement technique with standardization of the SPF opening in this study. An advantage of standardized anatomical landmarks is that measurements can be performed repeatedly in a reliable and comparable manner.

In terms of S-L, our NSF is in accordance with previously described lengths in the literature [14, 22, 24]. Pinheiro-Neto et al. [14] found a slightly larger S-L of 72 mm. However, they added during their evaluation of length an arbitrary 6 mm to allow for possible tissue contraction. Without the addition of these 6 mm, their calculated S-L is in agreement with our calculated S-L. Because our clinical experience is that NSF contraction is not significant, we did not add additional length to the NSF.

In our study, the calculated CBCT NSF-S was 19.8 cm^2. Other studies calculated NSF surfaces in a range between 22.6–27.7 cm^2 [14, 24]. Although these studies claimed a larger NSF surface, the method for measuring the surface using a combination of measurements is not precisely revealed, thereby making comparisons not very reliable. Moreover, these studies only used CT data to calculate the surface where we found strong positive correlations between CBCT NSF reconstructions and anatomical dissections. Measurements on 3D CBCT surface images are accurate and a relative error less than 1 % is seen [25, 26].

Compared to CT, CBCT provides relatively low-dose high spatial resolution visualization of high-contrast structures [27, 28]. It has been shown that CBCT is sufficient for the evaluation of vascular supply during intra-arterial chemotherapy for head and neck tumors [29, 30]. The complex anatomy of the vascular NSF pedicle makes it an attractive target for high spatial resolution imaging. However, visualization of the pedicle and its branching in vessels with a very small diameter failed because the quality of vessels in cadaver heads is not comparable to humans.

Previous studies conclude that the NSF is adequate to cover the entire anterior skull base [1, 3, 11, 14]. In these studies, the planum sphenoidale is not part of the anterior skull base. Whether it is possible to cover the entire skull base with the NSF, it matters whether the planum sphenoidale belongs to the anterior skull base. The posterior frontal sinus wall forms the anterior border of the ventral skull base. The lesser wings of the sphenoid sinus, connected by the planum sphenoidale, and the anterior clinoid processes form the posterior border of the anterior cranial fossa [31]. If in this study the NSF was positioned in front of the planum sphenoidale, which means from the anterior sphenoid sinus wall along the skull base toward the frontal sinus, the NSF also reached the posterior frontal sinus wall. However, the NSF length was not large enough to cover the entire skull base from the sella along the planum sphenoidale toward the posterior frontal sinus wall. To confirm this result, we additionally measured the skull base in the midsagittal plane of the CBCT, using P-SPF as reference. In all cadavers, the NSF was large enough to cover the skull base from the anterior sphenoid sinus wall to the posterior frontal sinus wall (69.9 mm [59.7–74.7]), but too small to cover the entire anterior skull base including the planum sphenoidale (86.2 mm [80.7–94.15]).

The posterior frontal sinus wall presents higher risk of failure in covering [11]. This is in accordance with our result that a skull base defect at the level of the anterior ethmoid sinuses presents a critical point for covering with an NSF. If the NSF was positioned from the sella along the skull base toward the frontal sinus, the NSF reached only partially into the anterior ethmoidal sinuses. Preoperative calculation of the NSF dimensions can help to decide if the NSF is sufficient to cover a skull base defect. If there is even a whisper of doubt, it is better to choose a different reconstruction method. Failure in creating an adequate reconstruction harbors the risk of complications, comprising CSF leaks and meningitis [32]. A postoperative CSF leak rate of 6 % is described because the NSF was deficient along the anterior-most part of the defect [9]. Moreover, the operative time increases unnecessary when time is used for NSF harvesting while it is not usable [7]. More importantly, undue damage to septal mucosa and olfactory

fibers can potentially lead to postoperative morbidity [7]. To prevent failure, it is recommended to overestimate the NSF size and to trim it if needed [1]. However, clinical experience shows that the NSF is often made too large during surgery. In these situations, especially the anterior septal mucosa is unnecessarily damaged with crusting as a consequence negatively affecting the patients quality of life (Qol) 6–15 weeks postoperatively [3, 12, 13, 33]. This study shows that a maximum NSF length was not necessary for covering the posterior ethmoid sinuses or sellar region. Anticipating on more posterior located defects, preoperative analyses using CBCT can be helpful in planning a limited and customized NSF in an attempt to spare septal mucosa. In the concept of minimal invasive surgery, this can benefit the patients' postoperative complaints.

It must be noted that our data is based on a cadaveric study, which is not completely comparable to the clinical setting. The information gathered in the present cadaveric study is of great practical value. However, a future research is necessary to study whether the suggested method of preoperative planning can be implementable in the clinical setting.

Conclusion

Cone beam computed tomography is a valuable technique for calculating NSF dimensions. Strong positive correlations were found between CBCT NSF reconstructions and anatomical dissections. The NSF reach for covering the anterior skull base depends on positioning. This cadaveric study encourages preoperative planning of a customized NSF, in an attempt to spare mucosa. In the concept of minimal invasive surgery, this can benefit the patients' postoperative complaints.

Acknowledgments We thank Klaas van Linschoten, Peter Veldman and Steve Oosterhoff of the section Anatomy, Ruud Kortekaas of the Department of Neuroscience and Minke van den Berge for help and (statistical) support.

Conflict of interest None.

References

1. Hadad G, Bassagasteguy L, Carrau RL, Mataza JC, Kassam A, Snyderman CH, Mintz A (2006) A novel reconstructive technique after endoscopic expanded endonasal approaches: vascular pedicle nasoseptal flap. Laryngoscope 116:1882–1886
2. El-Sayed IH, Roediger FC, Goldberg AN, Parsa AT, McDermott MW (2008) Endoscopic reconstruction of skull base defects with the nasal septal flap. Skull Base 18:385–394
3. Kassam AB, Thomas A, Carrau RL, Snyderman CH, Vescan A, Prevedello D, Mintz A, Gardner P (2008) Endoscopic reconstruction of the cranial base using a pedicled nasoseptal flap. Neurosurgery 63:ONS44–ONS52 (Discussion ONS52–3)
4. Patel MR, Taylor RJ, Hackman TG, Germanwala AV, Sasaki-Adams D, Ewend MG, Zanation AM (2013) Beyond the nasoseptal flap: outcomes and pearls with secondary flaps in endoscopic endonasal skull base reconstruction. Laryngoscope 124:846–852
5. Pinheiro-Neto CD, Snyderman CH (2013) Nasoseptal flap. Adv Otorhinolaryngol 74:42–55
6. Gagliardi F, Boari N, Mortini P (2011) Reconstruction techniques in skull base surgery. J Craniofac Surg 22:1015–1020
7. Eloy JA, Patel AA, Shukla PA, Choudhry OJ, Liu JK (2013) Early harvesting of the vascularized pedicled nasoseptal flap during endoscopic skull base surgery. Am J Otolaryngol 34:188–194
8. Harvey RJ, Nogueira JF, Schlosser RJ, Patel SJ, Vellutini E, Stamm AC (2009) Closure of large skull base defects after endoscopic transnasal craniotomy. Clin Artic J Neurosurg 111:371–379
9. Zanation AM, Carrau RL, Snyderman CH, Germanwala AV, Gardner PA, Prevedello DM, Kassam AB (2009) Nasoseptal flap reconstruction of high flow intraoperative cerebral spinal fluid leaks during endoscopic skull base surgery. Am J Rhinol Allergy 23:518–521
10. Peris-Celda M, Pinheiro-Neto CD, Funaki T, Fernandez-Miranda JC, Gardner P, Snyderman C, Rhoton AL (2013) The extended nasoseptal flap for skull base reconstruction of the clival region: an anatomical and radiological study. J Neurol Surg B Skull Base 74:369–385
11. Pinheiro-Neto CD, Ramos HF, Peris-Celda M, Fernandez-Miranda JC, Gardner PA, Snyderman CH, Sennes LU (2011) Study of the nasoseptal flap for endoscopic anterior cranial base reconstruction. Laryngoscope 121:2514–2520
12. de Almeida JR, Snyderman CH, Gardner PA, Carrau RL, Vescan AD (2011) Nasal morbidity following endoscopic skull base surgery: a prospective cohort study. Head Neck 33:547–551
13. McCoul ED, Anand VK, Bedrosian JC, Schwartz TH (2012) Endoscopic skull base surgery and its impact on sinonasal-related quality of life. Int Forum Allergy Rhinol 2:174–181
14. Pinheiro-Neto CD, Prevedello DM, Carrau RL, Snyderman CH, Mintz A, Gardner P, Kassam A (2007) Improving the design of the pedicled nasoseptal flap for skull base reconstruction: a radioanatomic study. Laryngoscope 117:1560–1569
15. Hashimoto K, Arai Y, Iwai K, Araki M, Kawashima S, Terakado M (2003) A comparison of a new limited cone beam computed tomography machine for dental use with a multidetector row helical CT machine. Oral Surg Oral Med Oral Pathol Oral Radiol Endod 95:371–377
16. Halazonetis DJ (2005) From 2-dimensional cephalograms to 3-dimensional computed tomography scans. Am J Orthod Dentofacial Orthop 127:627–637
17. Ahmad M, Jenny J, Downie M (2012) Application of cone beam computed tomography in oral and maxillofacial surgery. Aust Dent J 57(Suppl 1):82–94
18. van Vlijmen OJ, Rangel FA, Berge SJ, Bronkhorst EM, Becking AG, Kuijpers-Jagtman AM (2011) Measurements on 3D models of human skulls derived from two different cone beam CT scanners. Clin Oral Investig 15:721–727
19. Fourie Z, Damstra J, Ren Y (2012) Application of cone beam computed tomography in facial imaging science. Shanghai Kou Qiang Yi Xue 21:220–231
20. Fourie Z, Damstra J, Schepers RH, Gerrits PO, Ren Y (2012) Segmentation process significantly influences the accuracy of 3D surface models derived from cone beam computed tomography. Eur J Radiol 81:e524–e530

21. Chiu CS, Clark RK (1991) Reproducibility of natural head position. J Dent 19:130–131
22. Shah RN, Surowitz JB, Patel MR, Huang BY, Snyderman CH, Carrau RL, Kassam AB, Germanwala AV, Zanation AM (2009) Endoscopic pedicled nasoseptal flap reconstruction for pediatric skull base defects. Laryngoscope 119:1067–1075
23. Rasband WS (1997–2014) ImageJ, U.S. National Institutes of Health, Bethesda, MD. http://imagej.nih.gov/ij/
24. Cheng F, Yin S, Djamaldine MS, Zhang W (2013) Endoscopic reconstruction skull base using pedicled nasoseptal flap and its anatomy measurement. Lin Chung Er Bi Yan Hou Tou Jing Wai Ke Za Zhi 27:741–744
25. Hassan B, Metska ME, Ozok AR, van der Stelt P, Wesselink PR (2010) Comparison of five cone beam computed tomography systems for the detection of vertical root fractures. J Endod 36:126–129
26. Stratemann SA, Huang JC, Maki K, Miller AJ, Hatcher DC (2008) Comparison of cone beam computed tomography imaging with physical measures. Dentomaxillofac Radiol 37:80–93
27. Kau CH, Richmond S, Incrapera A, English J, Xia JJ (2007) Three-dimensional surface acquisition systems for the study of facial morphology and their application to maxillofacial surgery. Int J Med Robot 3:97–110
28. Miracle AC, Mukherji SK (2009) Conebeam CT of the head and neck, part 1: physical principles. Am J Neuroradiol 30:1088–1095
29. Kakeda S, Korogi Y, Miyaguni Y, Moriya J, Ohnari N, Oda N, Nishino K, Miyamoto W (2007) A cone-beam volume CT using a 3D angiography system with a flat panel detector of direct conversion type: usefulness for superselective intra-arterial chemotherapy for head and neck tumors. Am J Neuroradiol 28:1783–1788
30. Ishikura R, Ando K, Nagami Y, Yamamoto S, Miura K, Pande AR, Yamano T, Hirota S, Nakao N (2006) Evaluation of vascular supply with cone-beam computed tomography during intraarterial chemotherapy for a skull base tumor. Radiat Med 24:384–387
31. Wachsmuth L (2004) Praktische Anatomie. Springer Verlag, Berlin
32. Harvey RJ, Smith JE, Wise SK, Patel SJ, Frankel BM, Schlosser RJ (2008) Intracranial complications before and after endoscopic skull base reconstruction. Am J Rhinol 22:516–521
33. de Almeida JR, Vescan AD, Gullane PJ, Gentili F, Lee JM, Lohfeld L, Ringash J, Thoma A, Witterick IJ (2012) Development of a disease-specific quality-of-life questionnaire for anterior and central skull base pathology–the skull base inventory. Laryngoscope 122:1933–1942